POAC'23
Glasgow, United Kingdom

Proceedings of the 27th International Conference on
Port and Ocean Engineering under Arctic Conditions
12-16 June 2023, Glasgow, United Kingdom

Forces associated with the initiation of ice movement events in the north Caspian Sea

McKenna, R.F.[1], Kadranov, Y.[2], Sigitov, A.[2] and Vernyayev, S.[2]

[1] R.F. McKenna Associates, Wakefield, QC, CANADA
[2] ICEMAN.KZ LLP, KAZAKHSTAN

ABSTRACT

The stability of the ice cover under the action of wind forces and water level changes is an important consideration in the north Caspian Sea. The initiation of movement for a stationary ice cover can be difficult to predict due to anchoring at shore, manmade islands, stamukhi and other grounded rubble features. Experience has shown that numerous factors, including water level changes due to wind surge, evolution of wind speed and direction, and state of the ice cover can influence this process. Periods of sustained warm temperatures can alter the ice cover sufficiently to promote ice movement, even in the absence of observable reductions in ice concentration.

Detailed data, both spatially and temporally, have been collected for the north Caspian Sea for recent years, documenting the state of the ice cover and many of the contributing metocean parameters. These data have been compiled for ice movement events in the 2015/2016 and 2020/2021 winter seasons to better understand the balance of environmental forces and resisting forces due to ice contact with the seabed and other obstacles.

A finite element model with a spatial resolution of 1 km has been exercised to model these events. The ice is represented as a cracked elastic material, and contacts with the seabed and obstacles are represented as fixed boundaries where the reaction forces are associated with ice failure or sliding. Spatially and temporally varying water surface elevations and wind stresses are modelled explicitly based on the event data. Focus of the modelling effort is on circumstances where the ice cover was initially stationary and subsequently moved under due to wind forcing. As modelled, ice movement events take place when the resisting forces and shore, artificial islands and stamukhi are exceeded, and when gap elements open.

KEY WORDS: Ice; Cover; Stability; Caspian Sea

INTRODUCTION

The finite element (FE) representation of the ice cover used in this paper is described in McKenna et al (2021) and McKenna and Crocker (2021), and its implementation for the present problem is described in McKenna et al (2023). The ice cover is modelled using elastic continuum elements and random pre-existing cracks are represented using gap elements that allow full motion when open and do not allow sliding when closed. Offshore islands, stamukhi and shore nodes are initially assigned as zero-displacement boundary conditions and subsequently allowed to displace according to the force constraints described in McKenna et al (2023).

The region considered in this paper is in the northeastern corner of the Caspian Sea, as shown by the dashed red line in Figure 1. The winter season, which typically lasts from two to four months, is characterized by a mobile ice cover that reaches a thickness of about 0.5 m. To assist with design and operational aspects of offshore oil and gas developments, an effort has been made in recent years to develop comprehensive winter hindcasts of ice and related parameters based on publicly available data (Vernyayev et al, 2023b). Key parameters are given in Table 1. The spatial resolution of the database is 1 km, although input data from satellite images and other sources is variable. The ERA5 hindcast wind grid (ERA5, 2023) is shown in Figure 1, as are sub-regions with generally consistent ice regimes represented by the three-letter codes.

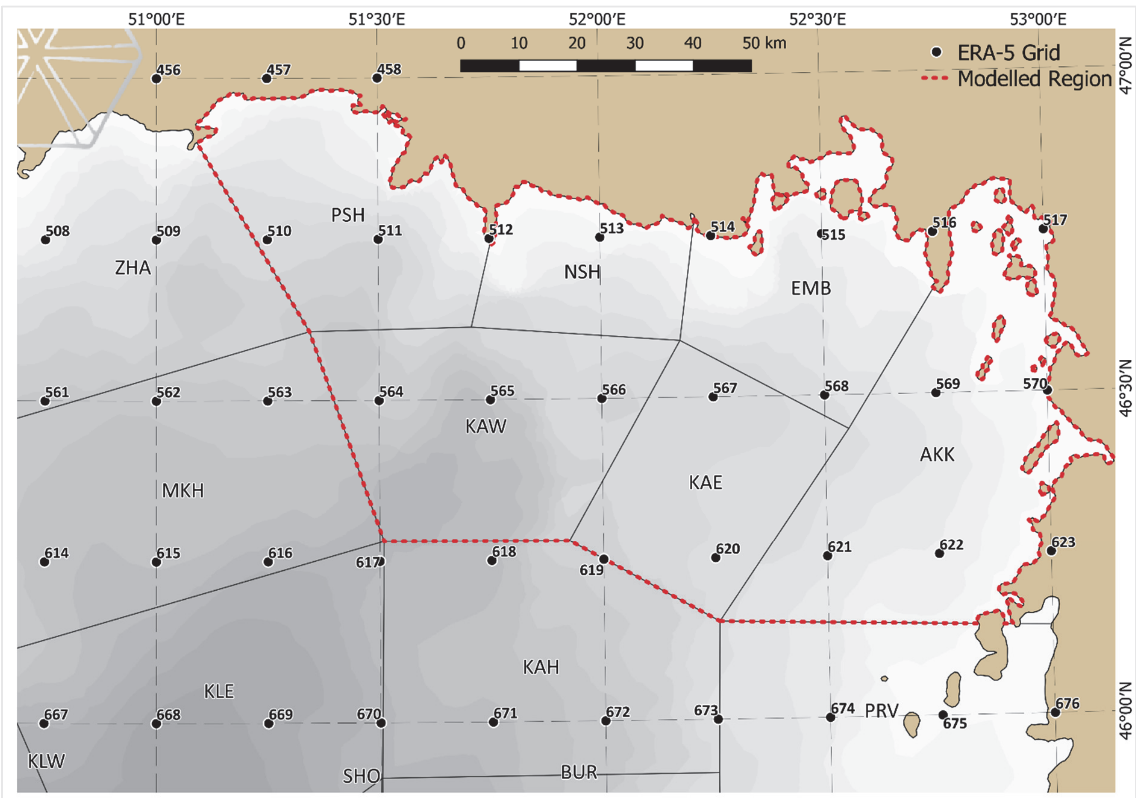

Figure 1 Modelled region of the north Caspian Sea

ICE REGIME IN THE NORTH CASPIAN SEA, 2015/2016 AND 2020/2021

This paper focuses on two winters, a mild one (2015/2016, with less than 250 FDD) and a moderate one (2020/2021, with about 625 FDD). These data are for the Kashagan East area, shown as KAE in Figure 1, a roughly 35 km x 35 km area that includes numerous man-made islands used for hydrocarbon production.

Table 1 Winter hindcast ice parameters

Parameter	Source	Spatial Resolution	Temporal Resolution
10 m wind speed/direction 2 m air temperature	ERA5	25 km (approx.)	Hourly
Ice concentration (3 thickest ice types)	Satellite imagery	1 km	Daily
Ice thickness (3 thickest ice types)	Satellite imagery, ice growth algorithm	1 km	Daily
Floe size (3 thickest ice types)	Satellite imagery	1 km	Daily
Ice drift	Ice buoys, satellite images, model predictions	Variable	Daily (or better)
Bathymetry	Public navigation charts, digitized by ICEMAN.KZ	1 km	-
Water level	Peshnoi gauging station	-	Daily
Relative ice strength	Accumulated 5-day air temperature	1 km	Daily
Ice cover mobility	Repeat satellite imagery	1 km	Daily
Stamukha location and footprint	Repeat satellite imagery	10 m (footprint) Variable (position)	Daily

The 2015/2016 ice season at KAE lasted from early January until late February and the maximum thermally-grown ice thickness was about 0.25 m. The total ice concentration only approached 10/10 for about one quarter of the ice season was never stable during this winter season. In contrast, the 2020/2021 ice season lasted from mid-November to the beginning of April and the maximum ice thickness due to thermal growth reached about 0.5 m. The total concentration in this area was 10/10 or nearly so throughout much of the winter and there were about ten periods of varying duration (about 1 to 10 days) when a portion of the ice cover in this area was mobile.

Twelve ice movement events were inferred from the hindcast database for the 2015/2016 and 2020/2021 winters, as listed in Table 2. Start day and duration were inferred from the state of the ice cover in the database, primarily using the “mobile” and “compacting” designations derived from repeat satellite imagery (see Sigitov et al, 2023 for definitions). The days are cumulative from January 1 of 2015 and 2020 (i.e. these were Day 0). Winds listed in Table 2 are average 10 m values over the area based on ERA5 data, while water levels (based on KazHydroMet, 2023) are deviations from the 60-day running mean. Positive changes in water level typically occur when the wind direction is from the SW quadrant and negative changes when from the NE quadrant. While all events were associated with increases in the wind speed, often reaching over 10 m/s, there does not appear to be a pattern of increasing water level. Peak water levels tend to lag the time of peak wind speeds by about 12 h.

While space prohibits a detailed description of all events, the sequence of mobility characterizations for Event 6 is shown in Figure 2 and the sequence for Event 8 is shown in Figure 3. For Event 6, the ice was mostly stable for days 378 and 379, and the SW region became mobile progressively over days 380 and 381. For Event 8, the ice was mostly stable or stationary on day 401 and largely mobile or compacting on day 402.

Except for ice cover mobility, all data described in Table 1 are used directly as input to the FE model. Observed ice mobility is used as a check on the FE model results. Although it is acknowledged that some ice strength measure, independent of ice thickness, could be important for modelling the stability of the ice cover, relative strength derived from ERA5 air temperatures has not been applied in the present work.

Table 2 Partial list of ice movement events for 2015/2016 and 2020/2021 winters inferred from ice mobility data

Event	Winter	Start Day	Duration	Event Details
1	2015/2016	413	1 day	Compaction event 411.5 wind SE 6 m/s, w.l. dev. +0.1 m 412.875 wind S-NW 10.2 m/s, w.l. dev. +0.17 m
2	2015/2016	419	4 days	Break-up 418.667 wind ENE 2.9 m/s, w.l. dev. 0.0 m 419.5 wind E 6.6 m/s, w.l. dev. -0.07 m
3	2020/2021	326	1 day	Strip of mobile ice off edge of stationary ice 324 wind ESE 6.9 m/s, w.l. dev. -0.20 m 325 wind ESE 12.3 m/s, w.l. dev. -0.08 m
4	2020/2021	328	1 day	Area to S of Kashagan (KAE) moves 328.5 wind SSE 2.2 m/s, w.l. dev. +0.22 m 329.375 wind SSE 7 m/s, w.l. dev. +0.34 m
5	2020/2021	332	2 days	Large area of ice S of Kashagan (KAE) moves 332.125 wind S 5.3 m/s w.l. dev. +0.41 m 333.875 wind ESE 10.6 m/s, w.l. dev. +0.37 m
6	2020/2021	378	3 days	Large area of ice in SW region moves 378.125 wind ESE 6 m/s w.l. dev. +0.09 m 379.25 wind SE 15 m/s, w.l. dev. +0.15 m
7	2020/2021	387	1 day	Ice compacts against stationary ice 387 wind WSW 4.6 m/s, w.l. dev. +0.01 m 387.875 wind WSW-W 9.1-5.9 m/s w.l. +0.03 m
8	2020/2021	401	2 days	Ice compacts against stationary ice 401.75 wind WSW 5.4 m/s, w.l. dev. +0.11 m 402.25 wind W 14.2-10.6 m/s, w.l. dev. +0.21
9	2020/2021	412	2 days	Ice moving westward 412 wind NNE 7 m/s, w.l. dev. -0.23 m 414 wind NW 11.1 m/s, w.l. dev. -0.38 m
10	2020/2021	431	2 days	Ice moving eastward 430.25 wind SW 6.3 m/s, w.l. dev. +0.11 m 431.375 wind NW 11.6 m/s, w.l. dev. +0.11 m
11	2020/2021	439	4 days	Westward movement over a large area 439 wind ESE 4.5 m/s, w.l. dev. -0.20 m 441 wind ESE 14.5 m/s, w.l. dev. -0.09 m
12	2020/2021	446	5 days	Break-up 447 wind SE 4 m/s, w.l. dev. +0.24 m 448.75 wind E 13.3 m/s, w.l. dev. +0.11 m

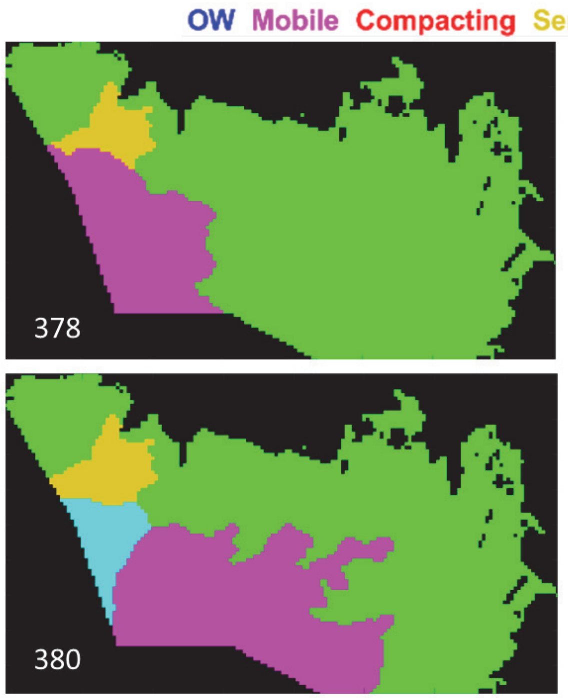

Figure 2 Winter 2020/2021 Event 6 daily ice mobility (colour interpretations in title)

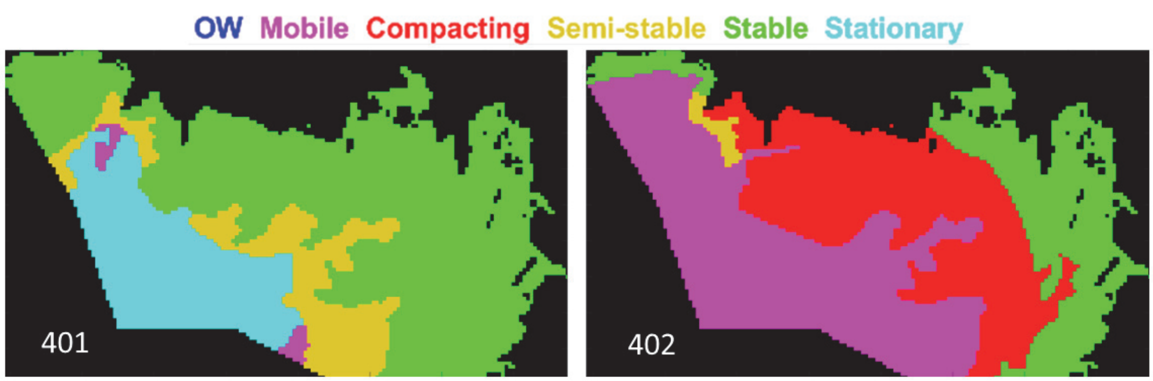

Figure 3 Winter 2020/2021 Event 8 daily ice mobility (colour interpretations in title)

FINITE ELEMENT REPRESENTATION OF THE ICE COVER

The ice grid data summarized in Table 1 are specified at a 1 km spatial resolution. For the FE analysis, each grid square is modelled as a pair of two-dimensional triangular constant strain elements using a plane stress assumption (no stress in the vertical direction). Since cracks are always present in the ice cover, a gap element is placed along the face of each continuum element and a gap node is placed at each vertex, as described in McKenna et al (2023). Each gap node is common to the surrounding gap elements and boundary conditions are only applied to the gap nodes. The gap elements are given a random orientation by adding a random component to all node locations. The FE grid has an E-W range of 158 km and a N-S range of

93 km, and consists of 17722 continuum elements, 53166 gap elements, 53166 nodes at the vertices of continuum elements and 9306 gap nodes.

The bathymetry of the Caspian Sea with a 1 km grid resolution has been interpolated to the FE node positions. In the western part of the region, maximum water depths reach about 7.0 m in 2015/2016 and 6.3 m in 2020/2021 since the average winter water level is decreasing over time in this area. Shore boundary conditions are assigned to 667 gap nodes that are on the edge of the area and where the sea floor elevation exceeds -0.75 m (CD, Caspian Datum). Twenty artificial island and submerged berm locations from offshore oil and gas development are placed at the closest node in the FE grid, and a plan diameter, including protection berms, has been assigned for use in the reaction force calculations. Displacements along the W and S boundaries of the modelled region are not prescribed and are left free to move. Particularly for winds from the W-SW-S sectors, this assumption may not be a good one when there is ice present adjacent to these boundaries.

The stamukha locations at the start of a FE simulation are also assigned to the closest node, and there can be as many as 100 stamukhi over the area covered by the FE grid at any one time. While the plan diameter of each stamukha has been estimated from the satellite images, the average freeboard has not been measured. For resistance calculations, the average total thickness of each stamukha is assumed to be 1.5 times the 60-day moving average water depth at that location.

The ERA5 winds are provided on an hourly basis at grid points that are approximately 20 km apart E-W and 28 km apart N-S (Figure 1) and interpolated to the continuum element centroids.

Ice thickness is used in a couple of different ways in the analysis – as a multiplier on the stiffness of the continuum and gap elements, and as a parameter in the failure mechanisms at shore, islands and stamukhi. The latter effect is generally more significant in the FE model results. The daily grid values of ice thickness are available for three different ice concentrations and the net effect from a mechanical standpoint is likely to be some composite of the three. At artificial islands and stamukhi, which are for the most part less than the grid dimension (except for the large D-island production facility), a weighted average thickness of all the ice at that location is assumed. A weighted average thickness is also assumed for the continuum elements. For the shore nodes, each of which represents about 1 km in shoreline length, a weighted average of the thinnest 1/10 of the ice cover is assumed because the ice deformation tends to be concentrated in areas where the ice is thinnest. For the gap element stiffness, the weighted average of the thinnest 1/10 of the ice cover is also used. This choice is made to reflect the fact that compressive deformation or strain in a natural ice cover tends to be localized rather than evenly distributed. Compressive failure due to ridging or rafting is not modelled and using the thinnest ice for the gap node stiffness is a way of accounting for this in part.

SIMULATION OF ICE DISPLACEMENT EVENTS

FE simulations were run for each of the ice movement events shown in Table 2. The various runs covered time periods ranging from 12 h and 48 h. Since wind is the primary driving force on the ice cover, the runs typically started with wind speeds below 5 m/s and ended when the speed reached a maximum value (up to about 15 m/s) or to capture a change in direction after the maximum was reached. While some of the events involved increasing water levels, the changes over the duration of the runs never reached more than about 0.15 m.

The FE run results were first interpreted by plotting the time series, as shown in Figure 4 for Event 6. The top four plots describe the wind and ice environments from the database. The fifth and sixth plots show displacements and reaction forces for all island gap nodes and for some of the stamukha and shore nodes. The displacements and forces for the shore nodes are generally small because of load sharing. As the wind speed increases, the reaction forces rise until the limiting forces are reached for prescribed displacement nodes. Once the limiting force is reached, the node is allowed to displace and thereby accommodate the excess wind energy. Increasing displacements are an indication that this is happening, whereas a levelling of the displacement trace is an indication that the applied winds have decreased. Decreasing reaction forces are also a sign of either decreasing wind speed or a change in direction that might shelter an island or stamukha from the ice cover upwind.

The bottom plot in Figure 4 shows the total wind force over the modelled area and the sum of all reaction forces at the prescribed nodes. The total wind force starts to deviate from the sum of the reaction forces at a simulation time of 5 h, and then deviates significantly at a time of about 9 h and a wind speed of 8.9 m/s. At a simulation time of 18 h, when the wind force deviation from the reaction force has levelled out, the wind speed has reached 13.8 m/s. Based on the second and third plots in Figure 4, the wind direction for Event 6 was ESE and the water level deviation from the 60-day mean was relatively modest.

Clearly, the ice displacements shown in Figure 4 are smaller than would be expected in practice and the intent is not to represent these accurately. The elastic constants for the continuum and gap elements are chosen primarily to make the explicit time integration of the ice mechanics numerically stable and efficient. Other models exist for estimating drift speeds once the ice cover is in motion and no attempt has been made to deal with that situation here.

Another way of interpreting the FE runs involved a spatial representation of the FE grid and open gap elements at selected points in time, as shown for Event 6 in Figure 5 (simulation time 9 h) and Figure 6 (simulation time 18 h). For the duration of this event, the wind direction was steady from ESE and open gaps are seen downwind of the stamukha and offshore islands. Open gaps are indicative of ice regions where ice movement is likely. A region without gaps upwind of a region with open gaps, but without any islands or stamukhi in between, is also likely to be mobile. After the average wind reached 13.9 m/s at a time of 18 h, the number of open gap elements also increased over a wider area in Figure 6, an indication of increased likelihood of ice mobility. Although the spatial representation of ice cover displacements was also consulted, the open gaps appear to be a better indicator of ice mobility. With reference to Figure 2 (observed changes from Day 379 to 380) and the top plot in Figure 4, the model also appears to have modelled widespread mobility sooner than observed in the data.

Many of the ice events modelled involve N-NE-E-ESE winds that cause the ice to pull away from the N and E shores of the modelled region. Event 8, shown in Figures 7 and 8 involves WSW and W onshore winds causing compaction of ice in parts of the region. Based on the difference between the total reaction and wind forces in Figure 7, ice movement over a broad region is initiated between simulation times of 9 h (wind 6.7 m/s) and 15 h (wind 14.1 m/s). In Figure 8, small areas with open gaps are found downwind of all islands and stamukhi but there is no widespread gap opening except at the NW corner of the region (where the free boundary condition is not likely to be appropriate).

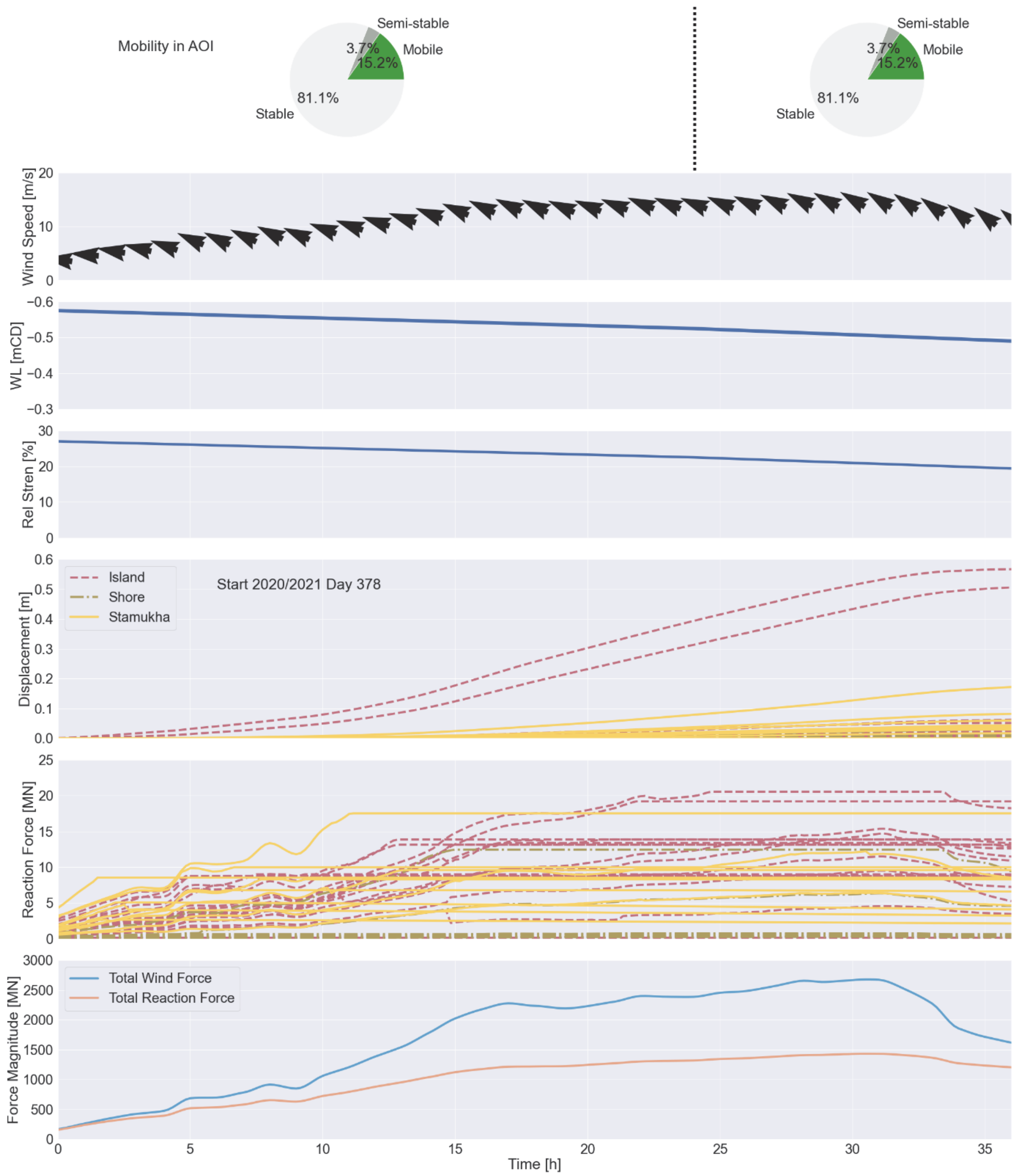

Figure 4 Time series for Event 6 (Tables 2,3): the top four plots show proportion of ice cover that is mobile, wind speed/direction, water level deviation from 60-day running mean and relative ice strength from the database; the bottom three plots show modelled displacements and reaction forces at offshore islands, some stamukhi and some shore nodes, as well as the total wind force and the sum of the reaction forces at nodes with prescribed displacements.

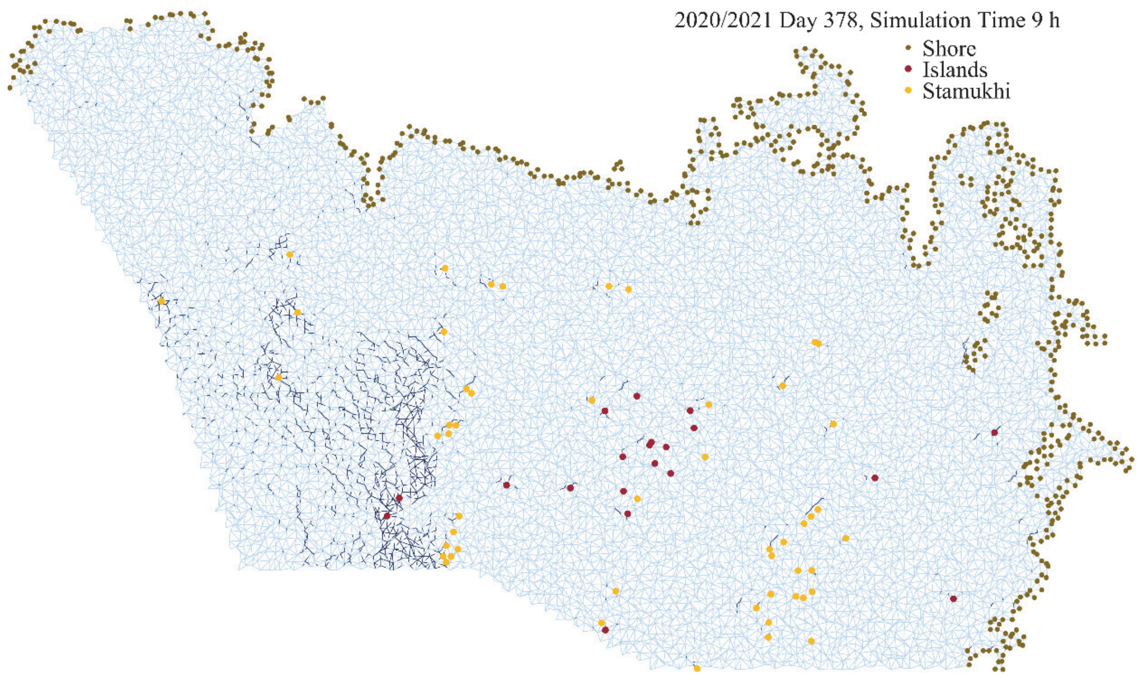

Figure 5 Open gap elements for 2020/2021 start day 378 (Event 6), simulation time 9 h. The FE grid as well as offshore island, stamukha and shore node positions are shown.

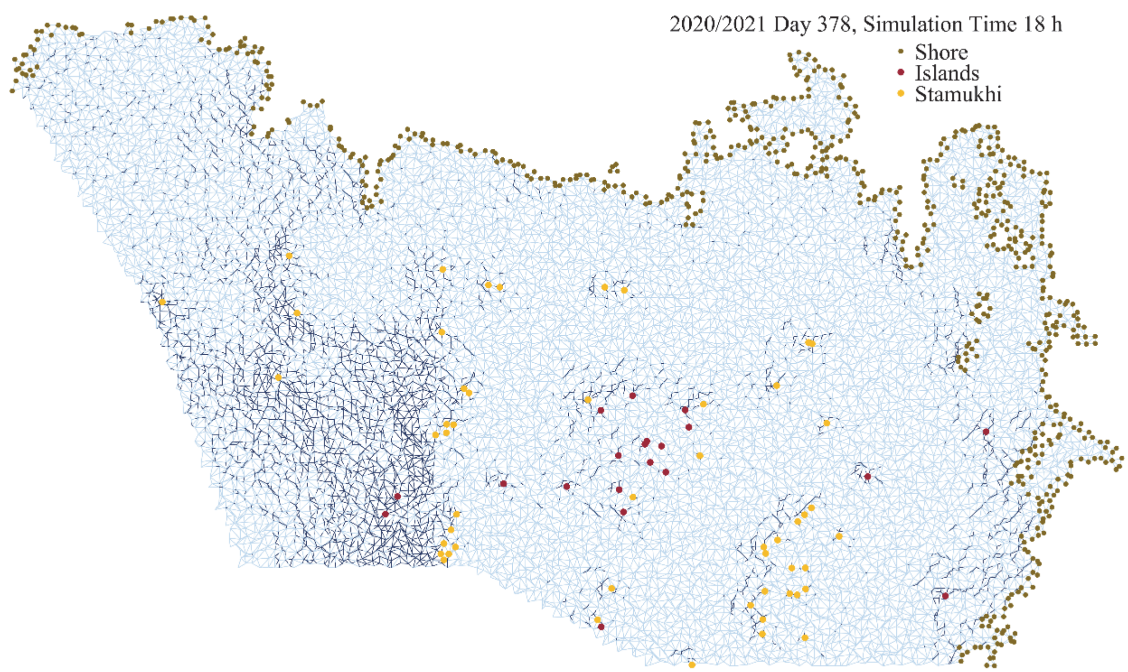

Figure 6 Open gap elements for 2020/2021 start day 378 (Event 6), simulation time 18 h.

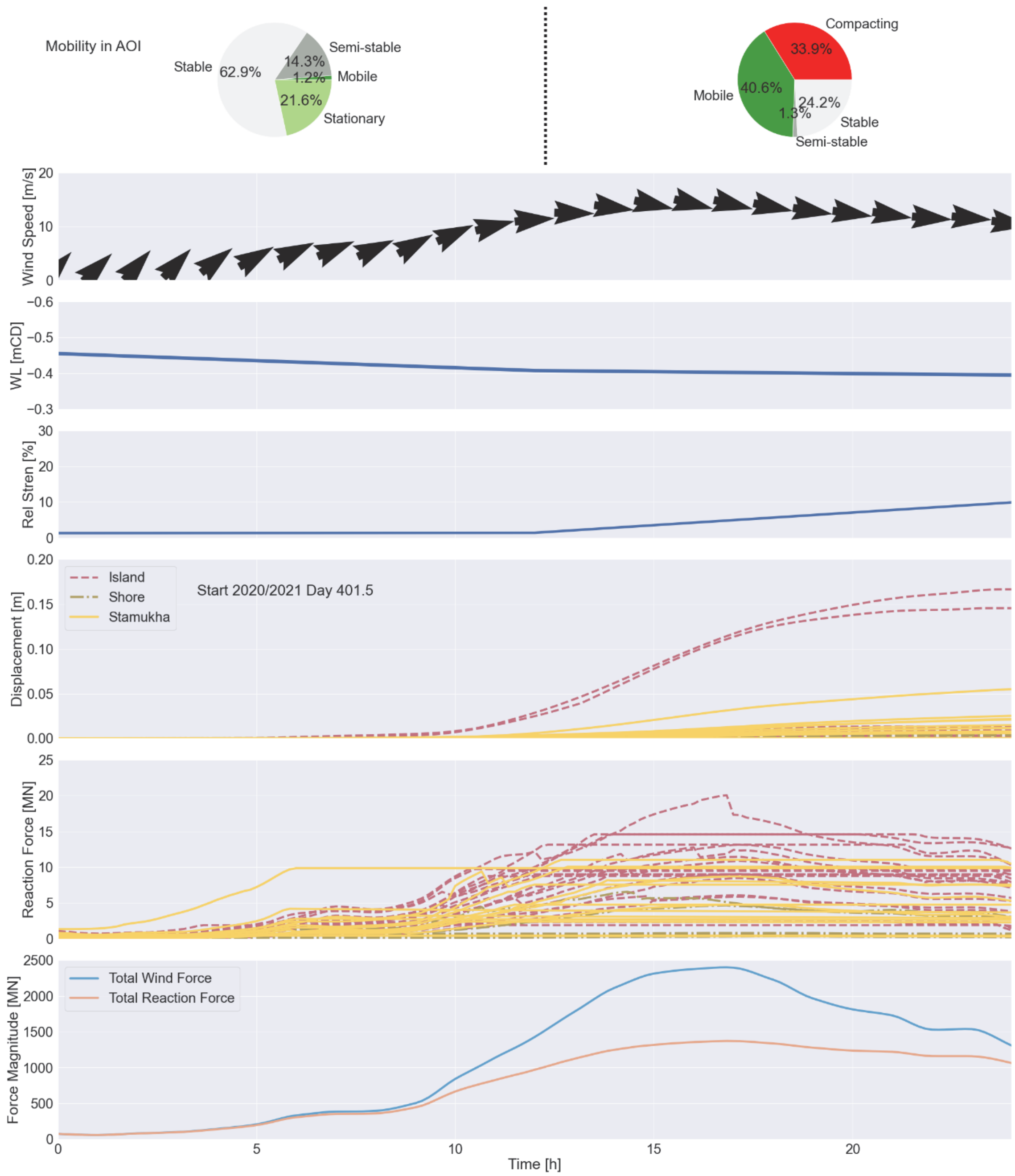

Figure 7 Time series for Event 8 (Tables 2,3): the top four plots show proportion of ice cover that is mobile, wind speed/direction, water level deviation from 60-day running mean and relative ice strength from the database; the bottom three plots show modelled displacements and reaction forces at offshore islands, some stamukhi and some shore nodes, as well as the total wind force and the sum of the reaction forces at nodes with prescribed displacements.

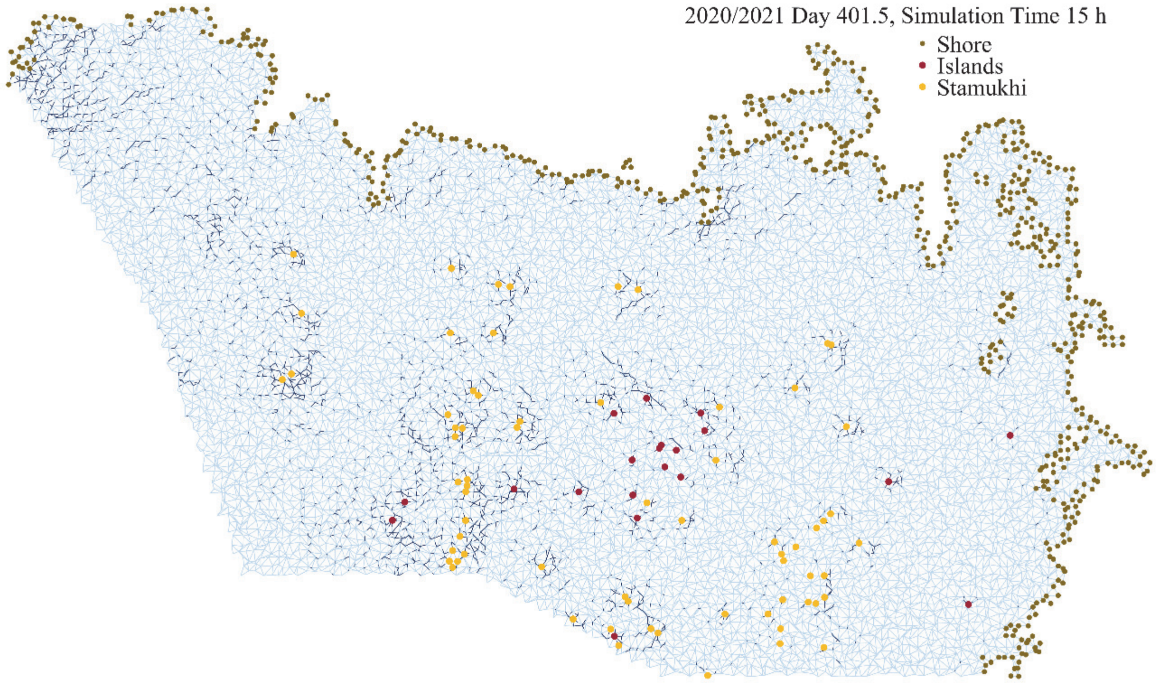

Figure 8 Open gap elements for 2020/2021 start day 401.5 (Event 8), simulation time 15 h

The above FE run results and the remaining ones are summarized in Table 3. The start of the ice movement event is based primarily on the average wind speed over the region at the simulation time when the total wind force starts to deviate significantly from the total reaction force. The full mobility status was confirmed by verification that the wind/reaction force deviation was accompanied by a regional increase in the density of open gap elements. The last column of Table 3 also provides some indication of how the modelled region of mobile ice matches the observed data for these events (e.g. Figures 2,3). A complementary empirical approach to wind thresholds for ice movement events involving wind direction, initial stability of the ice cover and relative strength is described in Vernyayev et al (2023a).

The FE model is intended to simulate an initially stationary and essentially continuous ice cover. For circumstances where large areas of open water are present, the solution may not be very accurate even if the solution is stable numerically. For some of the events, many gap elements opened soon after the start of the simulation, indicating that the ice can move readily, even for wind speeds less than 5 m/s. A better way to model these specific circumstances could potentially be addressed in future.

CONCLUSIONS AND DISCUSSION

A FE model has been developed for assessing the stability of an ice cover under wind actions. Of specific note is the development of special displacement boundary conditions where the nodes are allowed to slip when specified reaction forces are exceeded at shore, stamukhi and small offshore islands (McKenna et al, 2023). This model has been applied to twelve events for the north Caspian Sea over two winters derived from a hindcast database (Vernyayev et al, 2023b). While the idea of apportioning applied forces to boundary nodes is simple, this application is completely novel. The actual position of small offshore islands and grounded ice rubble features is represented, and the resistance to applied wind forces depends on water depth variations. The model also accounts explicitly for existing cracks using gap elements, which effectively allows the representation of an ice material behaviour with little or no tensile strength.

Table 3 Interpretation of simulated FE ice movement events for 2015/2016 and 2020/2021 winters

Event	**Run Year / Start Day / Duration**	**Start of Mobile Event**	**Full Mobility**	3x3 schematic of subregions with mobility observed but not modelled, correctly modelled and not observed but modelled
1	2015 Day 411.5 33 h	SSW 5.8 m/s 3 h	SSW 5.8 m/s 3 h	
2	2015 Day 418.75 24 h	ENE 4.8 m/s 3 h	ENE 6.6 m/s 9 h	
3	2020 Day 324 36 h	ESE 6.9 m/s 0 h	ESE 11.6 m/s 21 h	
4	2020 Day 328.5 30 h	SSE 4.3 m/s 6 h	SSE 5.8 18 h	
5	2020 Day 331.75 36 h	SE 6.8 m/s 15 h	ESE 8.3 m/s 30 h	
6	2020 Day 378 36 h	ESE 8.7 m/s 9h	ESE 13.8 m/s 18h	
7	2020 Day 387 18 h	SW 6.9 m/s 6h	SW 8 m/s 9h	
8	2020 Day 401.5 24 h	WSW 6.7 m/s 9 h	W 14.1 m/s 15 h	
9	2020 Day 412 48 h	NNE < 7 m/s 1 h	NE,NNW 9m/s 15 h, 42 h	
10	2020 Day 430.25 30 h	SW 10 m/s 24 h	SW 11.5 m/s 27 h	
11	2020 Day 439.125 48 h	ESE 9.5 m/s 24 h	ESE 13.3 m/s 39 h	
12	2020 Day 447 42 h	ESE 5.8 m/s 3 h	SE 10 m/s 21	

Ice movement events in the north Caspian Sea can typically last for a few hours to a few days. For practical reasons, focus in the FE simulations has been on generally increasing wind speeds, which likely initiate the ice motion even though the entire duration of the events is not always represented. While the modelled wind speed thresholds associated with local and regional ice movement events typically ranged from 5 m/s to 15 m/s (which is in line with observations, Vernyayev et al, 2023a), it is emphasized that the initiation of ice motion is a very complex issue, regardless of the ice environment.

The results presented in the paper are based on initial estimates of the parameters of the loading models for islands, stamukhi and shore given in McKenna et al (2023). Further assessment of 2015/2016 and 2020/2021 events as well as those from other years could be used to calibrate the load models. In the shallow waters of the north Caspian Sea, partially-grounded rubble features frozen into the ice cover could be incorporated even though they are not identified as stamukhi in the satellite images. A purely elastic representation has been used for the ice continuum elements and the gap elements. While preliminary tests were made for smaller ice regions, the effect of this choice on load sharing could be investigated further.

REFERENCES

ERA5 [online] ERA5 hourly data on single levels from 1940 to present, available at: https://cds.climate.copernicus.eu/cdsapp#!/dataset/reanalysis-era5-single-evels?tab=overview [Accessed 01 March 2023]

KazHydroMet [online] Annual Caspian Hydrological Regime data from KazHydroMet, available at: https://www.kazhydromet.kz/ru/kaspiyskoe-more/ezhegodnye-dannye-o-rezhime-kaspiyskogo-morya [Accessed 10 January 2023]

McKenna, R., Crocker, G. and Loewen, A., 2021. A finite element model for the deformation of floating ice covers, *Cold Regions Science and Technology*, Vol. 182, https://doi.org/10.1016/j.coldregions.2020.103213

McKenna, R. and Crocker, G., 2021. Effective moduli for flexure of a floating ice cover due to temperature variations through the depth of the ice, in *Proceedings of the 26th International Conference on Port and Ocean Engineering under Arctic Conditions*, Moscow, Russia.

McKenna, R.F., Crocker, G.B. and Croasdale, K.R. 2023. Modelling ice cover stability in response to wind forcing, in *Proceedings of the 27th International Conference on Port and Ocean Engineering under Arctic Conditions*, Glasgow, U.K.

Sigitov, A., Kadranov, Y., Vernyayev, S. and Vernyayeva, I. 2023. Caspian Ice Cover Mobility, in *Proceedings of the 27th International Conference on Port and Ocean Engineering under Arctic Conditions*, Glasgow, U.K.

Vernyayev, S., Kadranov, Y. and Sigitov, A. 2023a. Caspian Ice Cover Destabilization Wind Threshold, in *Proceedings of the 27th International Conference on Port and Ocean Engineering under Arctic Conditions*, Glasgow, U.K.

Vernyayev, S., Kadranov, Y., Sigitov, A. and Vernyayeva, I. 2023b. Caspian Sea Ice Cover Hindcast Database, in *Proceedings of the 27th International Conference on Port and Ocean Engineering under Arctic Conditions*, Glasgow, U.K.